Void Detection in Foam with Knit Lines Using THz Pulse Interrogation

H. T. Banks [1]   and   N. L. Gibson [2]
Center for Research in Scientific Computation
North Carolina State University
Raleigh, NC 27695–8205

February 4, 2006

Abstract

We model electromagnetic interrogation of a polyurethane foam using the TE mode of the 2D Maxwell's equations reduced to the wave equation for a fixed frequency in the THz regime. The foam block target contains knit lines which are modeled by modifying the speed of propagation, i.e., by altering the index of refraction. We describe our efforts to estimate the dielectric constant in the knit lines, as well as in the surrounding foam, by use of the classical Clausius–Mossotti equation, assuming only a change in density. We compare the numerical simulations accounting for knit lines to those in which knit lines are neglected, each in the context of modeling reflections of plane waves in foam with voids.

1   Introduction

The problem we consider is the scattering of a THz plane wave in the possible presence of thin knit lines (i.e., layers of increased density) and voids (i.e., pockets of no density) inside a block of low density polyurethane foam, similar to BX-250, which was used on the Space Shuttle Columbia. The detection of voids inside the Sprayed on Foam Insulation (SOFI) belonging to the Thermal Protection System (TPS) is of critical importance to the NASA Return to Flight effort. In initial efforts, THz frequency waves have been shown to be particularly useful in foam interrogation [8]. However, the modeling of and data interpretation for the propagation of a THz pulse inside of a material which exhibits heterogeneous microstructures of sizes that are on the order of the wave length of the interrogating field is not straight–forward. In addition, there is presently a paucity of data on the dielectric properties of low density foam in the THz regime. The work in [9] begins to remedy this deficiency.

Previous efforts in THz interrogation of SOFI generally involved limited signal processing techniques such as peak–to–peak intensity ratio detection [3] and time of flight methods to determine the existence of material variations (see for example [10]). Such approaches do not take advantage of very much of the information potentially contained in the reflected signal. A physics–based model could be used to more accurately ascertain the geometric properties of an anomaly, such as size and depth, as well as to distinguish between a variation due to the presence of a void and a normal variation due the presence of knit lines. The corresponding information–rich experimental data are difficult to obtain since the amplitudes of reflections from low density materials are very low to immeasurable using currently available power sources at the THz frequency (e.g., see Figure 2 of [7]). The theory and computations herein, therefore, are in the nature a "proof of concept" and will hopefully serve as added justification and motivation for the development of more powerful generation devices.

Models utilizing polarization mechanisms have been previously investigated [1, 2], but matching the simulations to actual composite material experimental data has not yet been completely successful. Moreover, these models were expressed in only one spatial dimension and thus they do not allow for non-normally incident angles or non-coplanar interfaces. Previous models also did not explicitly account for the effect of knit lines, using instead an effective dielectric constant computed from observed time of flight measurements. The current effort employs a two dimensional model of the propagation of a THz pulse through a medium with curved knit lines and arbitrarily shaped voids. Because an appropriate model for the dispersion in this

---

[1]htbanks@ncsu.edu
[2]ngibson@ncsu.edu

1. REPORT DATE **04 FEB 2006**	2. REPORT TYPE	3. DATES COVERED **00-00-2006 to 00-00-2006**
4. TITLE AND SUBTITLE **Void Detection in Foam with Knit Lines Using THz Pulse Interrogation**		5a. CONTRACT NUMBER
		5b. GRANT NUMBER
		5c. PROGRAM ELEMENT NUMBER
6. AUTHOR(S)		5d. PROJECT NUMBER
		5e. TASK NUMBER
		5f. WORK UNIT NUMBER
7. PERFORMING ORGANIZATION NAME(S) AND ADDRESS(ES) **North Carolina State University,Center for Research in Scientific Computation,Raleigh,NC,27695-8205**		8. PERFORMING ORGANIZATION REPORT NUMBER
9. SPONSORING/MONITORING AGENCY NAME(S) AND ADDRESS(ES)		10. SPONSOR/MONITOR'S ACRONYM(S)
		11. SPONSOR/MONITOR'S REPORT NUMBER(S)
12. DISTRIBUTION/AVAILABILITY STATEMENT **Approved for public release; distribution unlimited**		
13. SUPPLEMENTARY NOTES		
14. ABSTRACT **see report**		
15. SUBJECT TERMS		

16. SECURITY CLASSIFICATION OF:			17. LIMITATION OF ABSTRACT	18. NUMBER OF PAGES **10**	19a. NAME OF RESPONSIBLE PERSON
a. REPORT **unclassified**	b. ABSTRACT **unclassified**	c. THIS PAGE **unclassified**			

type of media has not yet been determined, we here neglect this phenomena in favor of focusing our attention on the reflections and refractions at the interfaces. We note that while a dispersion mechanism may later be coupled to this model, the single dominant frequency aspect of this problem will likely lead to similar results in both modeling approaches. In particular, insomuch as dispersion models treat the index of refraction as frequency dependent, we may assume that the constant index of refraction used herein is fixed at the value associated with the dominant frequency mode of the interrogating pulse.

2   Model

For our domain we choose a square region ($0 \leq x \leq b, 0 \leq y \leq b$) consisting of a low density material with possible layers of higher density and pockets which are modelled as having zero density,i.e., voids. Figure 1 depicts a simulation with a schematic of two knit lines (represented by dashed lines) $1 \ mm$ from each other, each parallel to an approaching plane wave, and perpendicular to the direction of propagation. The far right boundary ($y = b$) is assumed to be metallic and therefore supra–conducting, thus simulating the aluminum backing of the SOFI on the shuttle external tank.
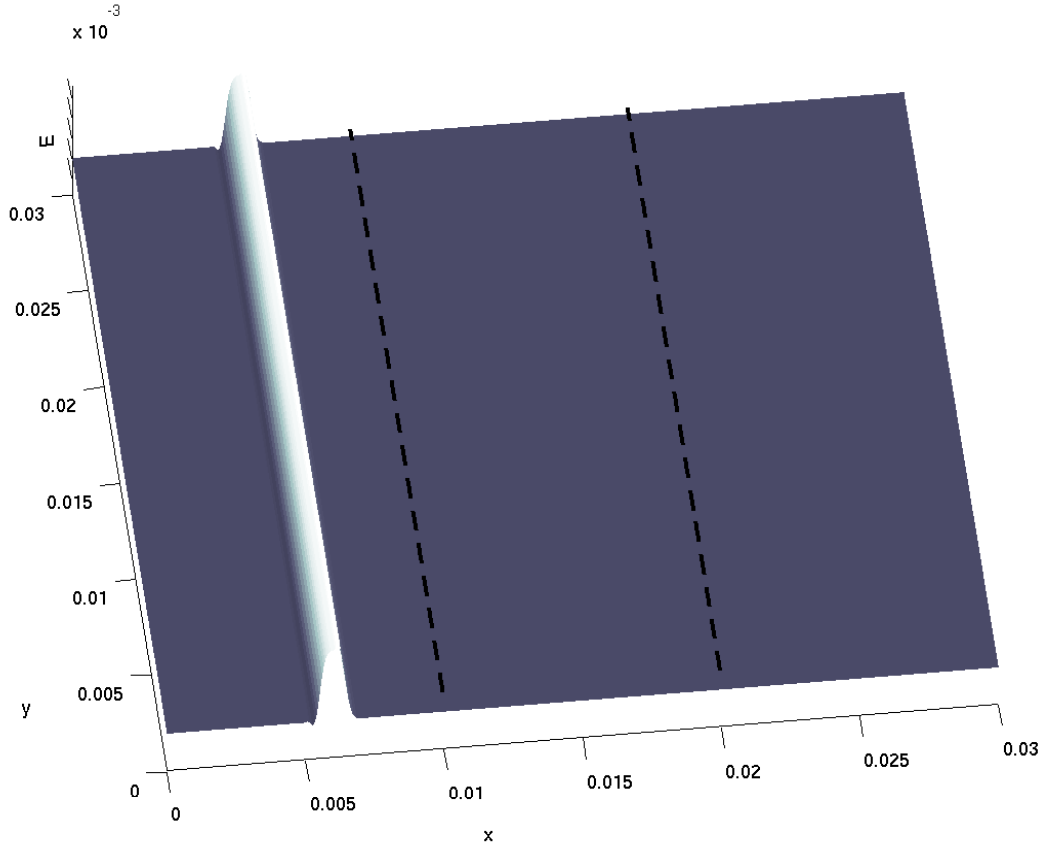

Figure 1: Simulation of plane wave approaching parallel knit lines.

We combine the TE mode of the two dimensional Maxwell's equations into one equation

$$\epsilon(\vec{x})\frac{\partial^2 E}{\partial t}(t,\vec{x}) + \nabla \cdot \left(\frac{1}{\mu(\vec{x})}\nabla E(t,\vec{x})\right) = -\frac{\partial J_s}{\partial t}(t,\vec{x}), \tag{1}$$

where $\vec{x} = (x, y)$, and $\epsilon(\vec{x})$ and $\mu(\vec{x})$ are the spatially dependent dielectric permittivity and magnetic perme-

ability, respectively. The corresponding speed of propagation is

$$c(\vec{x}) = \frac{c_0}{n(\vec{x})} = \sqrt{\frac{1}{\epsilon(\vec{x})\mu(\vec{x})}},$$

where c_0 is the speed in a vacuum and $n(\vec{x})$ is the index of refraction.

For our source current J_s we wish to simulate a windowed pulse, in this case a pulse that is allowed to oscillate for one half of one period and then is truncated. Although generators produce a curved, often spherical wave, we assume the target is sufficiently far from the generator (approximately 6 in) so that the wave is essentially planar when it reaches our domain of interest. We originate the pulse at $x = 0$, the left edge of our computational domain, and we model it in space as a delta distribution centered at $x = 0$. In order to have a smooth (in time) source we use a function of the form

$$J_s(t, \vec{x}) = \delta(x)e^{-((t-t_0)/t_0)^\gamma}, \tag{2}$$

where $t_0 = t_f/4$ when t_f is the period of the interrogating pulse. For example, if the frequency is $f = .2$THz, then $t_f = 1/f = .5 \times 10^{-11}$s. A reasonable value for the exponent is $\gamma = 4$.

2.1 Boundary/Initial Conditions

Our domain is defined to be the region $\vec{x} = (x, y) \in [0, b] \times [0, b]$. Thus to model a metallic backing behind the foam at $x = b$, we use reflecting (Dirichlet) boundary conditions

$$[E]_{x=b} = 0.$$

In order to have a finite computational domain, we impose first order absorbing boundary conditions at $x = 0$; these are modeled as

$$\left[\frac{\partial E}{\partial t} - c(\vec{x})\frac{\partial E}{\partial x}\right]_{x=0} = 0.$$

With these boundary conditions, ideally a normally incident signal passes out of the computational domain, and does not return, i.e., we force it to be absorbed by the boundary. Note that for signals that are incident at an angle, some reflection occurs. Lastly, to allow for propagation along the top and bottom boundaries ($y = 0$ and $y = b$), we use insulating boundary conditions

$$\left[\frac{\partial E}{\partial y}\right]_{y=0} = 0$$

$$\left[\frac{\partial E}{\partial y}\right]_{y=b} = 0.$$

We assume zero initial conditions so that

$$E(0, \vec{x}) = 0$$

$$\dot{E}(0, \vec{x}) = 0.$$

2.2 Modeling Knit Lines

To model the speed of wave propagation in the knit lines versus that in the material surrounding them, we must distinguish between the respective indices of refraction. However, we can currently only measure the *effective* index of refraction of the composite material, for example, by computing the "time of flight" in experiments. Thus we need to relate these three indices to each other in order to have accurate estimates for the propagation speed for use in simulations.

The effective index of refraction n_e can be estimated via the Clausius–Mossotti equation (see [6]), by assuming the total polarizability is the weighted sum of the two polarizabilities in each part of the material. In particular

$$\frac{n_e^2 - 1}{n_e^2 + 2} = \frac{\rho}{\rho_1}\frac{n_1^2 - 1}{n_1^2 + 2} + \frac{\rho}{\rho_2}\frac{n_2^2 - 1}{n_2^2 + 2}, \tag{3}$$

3

where ρ_i and n_i are the densities and index of refraction, respectively, in each part of the material, where part 1 corresponds to the low density region, and part 2 corresponds to the knit lines. The value ρ above is the total density given by

$$\rho = \nu\rho_2 + (1 - \nu)\rho_1 \tag{4}$$

if we assume that the knit lines comprise a certain volume fraction ν of the foam. Let the knit line density ρ_2 be some constant multiple of ρ_1 representing an increased density in the knit lines, i.e.,

$$\rho_2 = \beta\rho_1. \tag{5}$$

Substituting (4) and (5) into (3) we obtain

$$\frac{n_e^2 - 1}{n_e^2 + 2} = (\nu\beta + 1 - \nu)\left(\frac{n_1^2 - 1}{n_1^2 + 2} + \frac{n_2^2 - 1}{\beta(n_2^2 + 2)}\right). \tag{6}$$

If we further assume that the polarizability of the knit lines is equal to that of the low density region (this is in recognition that polarizability is a molecular characteristic and the molecules in the high density knit lines are not assumed to be significantly different than those in the low density regions; only the number of molecules is different), then we also have the following

$$\frac{n_1^2 - 1}{n_1^2 + 2} = \frac{n_2^2 - 1}{\beta(n_2^2 + 2)}, \tag{7}$$

and therefore,

$$\frac{n_e^2 - 1}{n_e^2 + 2} = 2(\nu\beta + 1 - \nu)\frac{n_1^2 - 1}{n_1^2 + 2}. \tag{8}$$

Thus, if n_e is estimated via experiments, n_1 can be determined using equation (8) with reasonable values of ν and β, and n_2 can in turn be calculated with equation (7).

Experiments have suggested, via time–of–flight measurements, a value for the effective index of refraction of $n_e = 1.03225 \pm 0.001$. The volume fraction ν can be estimated by noting the thickness of each knit line divided by the period in which the knit lines occur. For example, $0.5\ mm$ knit lines in each $0.5\ cm$ of foam corresponds to $\nu = .1$. The compression factor β is more difficult to measure, but experiments can be done to weigh samples with varying concentrations of knit lines to estimate the increase in density. An initial estimate based on pictures of SOFI under 20X magnification [4] is $\beta = 2.5$. Using the values $\beta = 2.5$ and $\nu = .1$, we can estimate the index of refraction in each part of the foam to be

$$n_1 = 1.01398 \tag{9}$$
$$n_2 = 1.03507. \tag{10}$$

If we compute the decrease in speed of a THz pulse due to the presence of knit lines by

$$p = \frac{1 - n_1}{n_e},$$

then (9) would correspond to an observed decrease in speed of 1.77%. Laboratory experiments have suggested that the decrease in speed is around 2%.

3   Results

We briefly describe here our techniques for solving the system described in (1) with the boundary and initial conditions outlined in Section 2.1. Simulations for the cases in which knit lines are ignored are compared to those where knit lines are described using the values estimated above.

3.1 Numerical Solution

We apply a Finite Element method using standard linear two dimensional ($Q1$) basis elements to discretize the model described by (1) in space. This results in nine-banded mass and stiffness matrices, M and S, respectively. We also have a contribution from absorbing boundaries which we denote by B. Thus our semi-discrete system for the vector of electric field values e is

$$M\ddot{e} + B\dot{e} + Se = f.$$

(Note that we have absorbed coefficients $\frac{1}{c^2}$ and $\frac{1}{c}$ into the definitions of M and B, respectively.)

For the temporal derivatives we use second order discretizations (centered differences) for both the first and second derivatives. After collecting all terms involving the updated time step into the left side of the equation, we have the following linear system

$$Ae_{n+1} = d, \tag{11}$$

where A contains multiples of M and B, and d depends on e_n and e_{n-1}, as well as S and f.

We ran numerical comparisons using various linear solvers including preconditioned conjugate–gradient and sparse LU factorization. The fact that the matrix A is stationary in time contributes to the fact that LU factorization performed better than any iterative method. However, the size of the problem that could be addressed was severely limited by the memory constraints when the LU factors exhibit fill–in. The iterative method on the other hand can be formulated using a matrix–free approach, thus freeing memory for representing a larger solution. Unfortunately, the computation time increases to an unacceptable level.

Therefore we prefer to use a mass–lumping approach where quadrature rules are applied to the basis functions to form mass and stiffness matrices which are diagonal. This results in an explicit linear system for (11). This system is simple to solve at each time step as it requires only division by the diagonal elements. There is an obvious loss in accuracy due to the approximate integration inherent in mass–lumping, but the increased efficiency allows for a finer discretization which can sometimes compensate. In fact, in our testing of small sample problems there is not a noticeable difference in accuracy between the three methods (when the computational times are comparable). However, a distinct difference is that for the LU method numerical error presented itself as oscillations preceding the signal, whereas for the mass-lumped problem, the oscillations followed the signal. Because the beginning of the reflection is important to determining the location and composition of a defect, we prefer for numerical error to trail the propagating wave and thus chose the lumped mass system for our simulations.

3.2 Simulations

We perform numerical simulations of a plane wave propagating through a material described by its index of refraction which determines the speed of propagation. We consider the presence of a void similar to what is seen in SOFI when a layer does not completely fill a recess formed in the previous layer, thus causing a pocket of air to be trapped. The void is modeled by taking its index of refraction to be that of free space ($n_0 = 1$).

Figure 2 displays snapshots in time of the propagation of a plane wave (the white band) incident on a void in the material. Here we neglect the specific properties of the knit lines by modeling the entire foam block using only the effective ("observed") index of refraction n_e. The reflection from the void is clearly seen in the second frame. This reflection expands out to form an oblong elliptical wave which eventually propagates back to the antenna where the signal is recorded with a receiver.

The simulations of the modeling approach proposed in this paper, namely the scenario where the knit lines are specifically modeled with their own index of refraction n_2 and the surrounding low density regions are described by n_1, are displayed in Figure 3. Reflections from the knit lines are apparent in the first frame. As in the homogeneous case above, the reflection from the void is again visible in the second frame. The interacting reflections are clearly more complicated in this scenario, as is the data collected by the receiver.
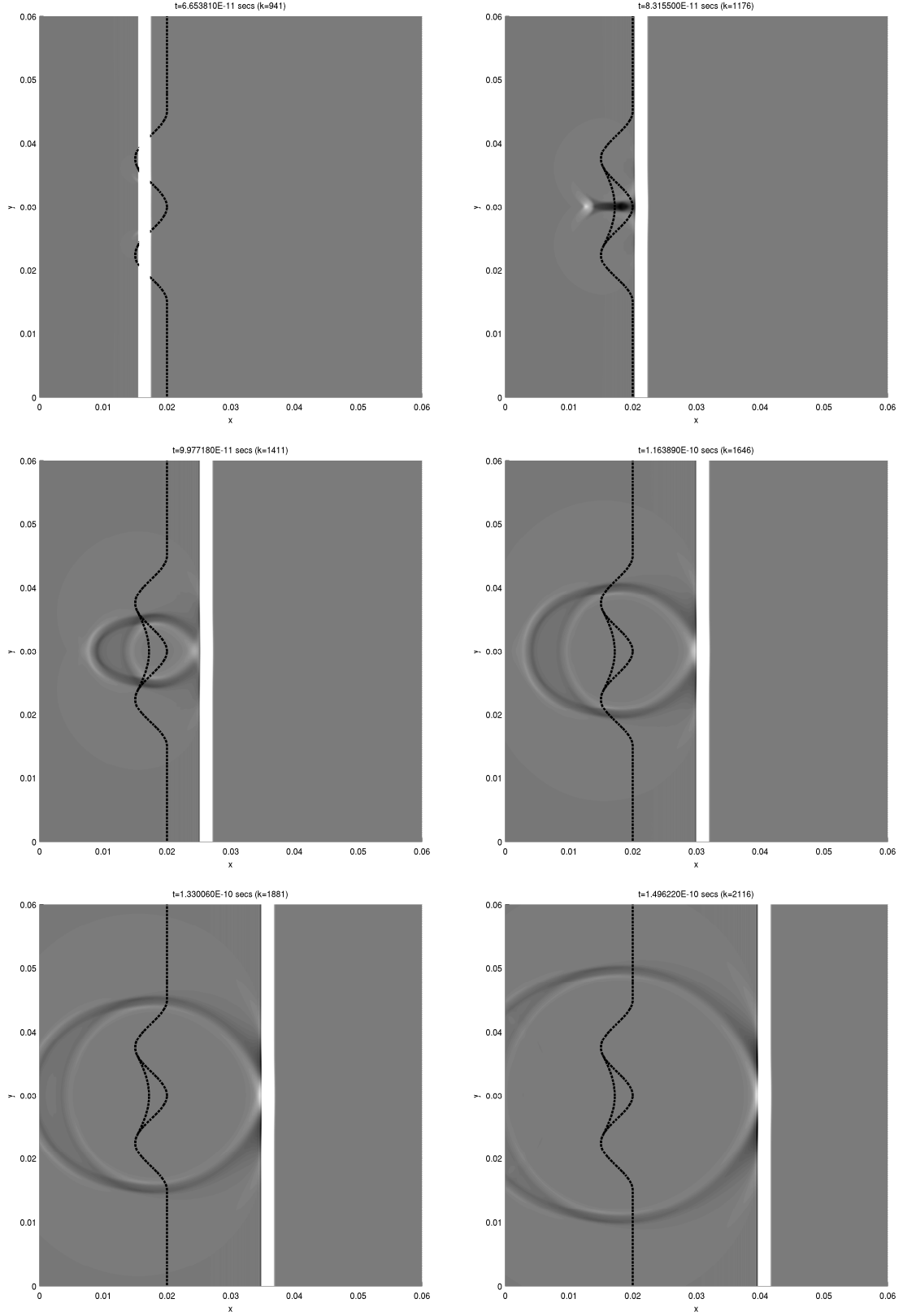
Figure 2: Surface plots of solutions for the case where the effective index of refraction is used in the low density part of the foam and in the knit lines (i.e., the presence of knit lines is ignored).
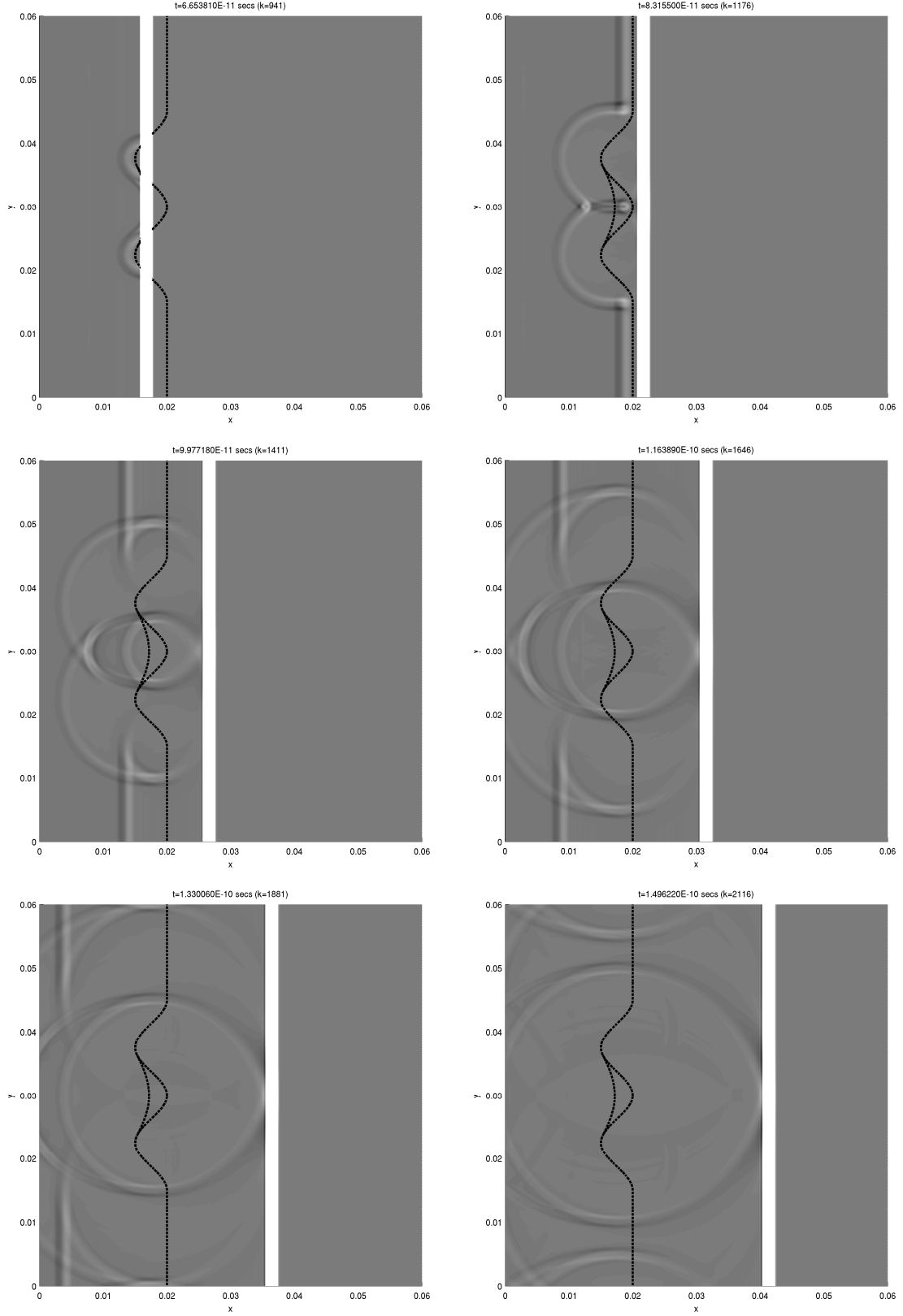
Figure 3: Surface plots of solutions for the case where the indices of refraction n_1 and n_2 are used in the low density part of the foam and in the knit lines, respectively (i.e., the presence of knit lines is not ignored).

Figures 4 and 5 depict the data collected over time at the receiver for the two different modelling approaches, respectively. In the main plot of each figure the magnitude of the reflection relative to that of the interrogating signal is apparent. The inset plot of each figure presents a magnification of the reflection from the void. There is a distinct difference in the structure of the two reflections. In particular, the reflection from the knit line is clearly visible in front of the reflection from the void in the second case. Note that the amplitude of the reflections in each case is roughly equivalent, while in the latter case the disruption to the electric field occurs for a longer duration.
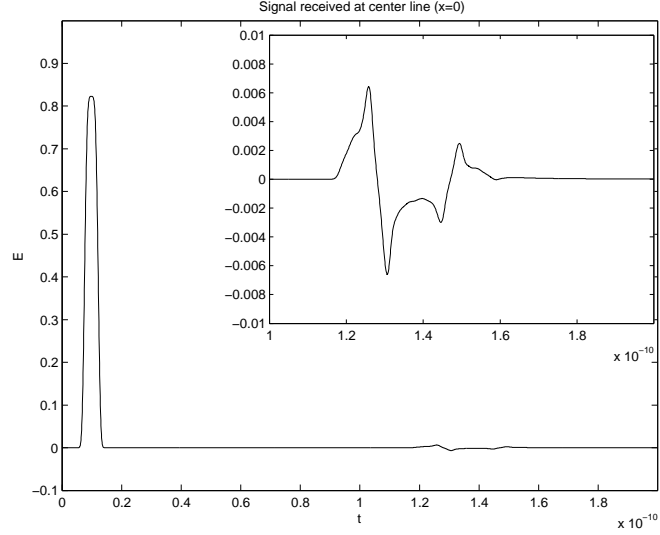

Figure 4: Signal received at $x = 0$ on the center line for the homogeneous case (the inset is a magnification of the reflection).
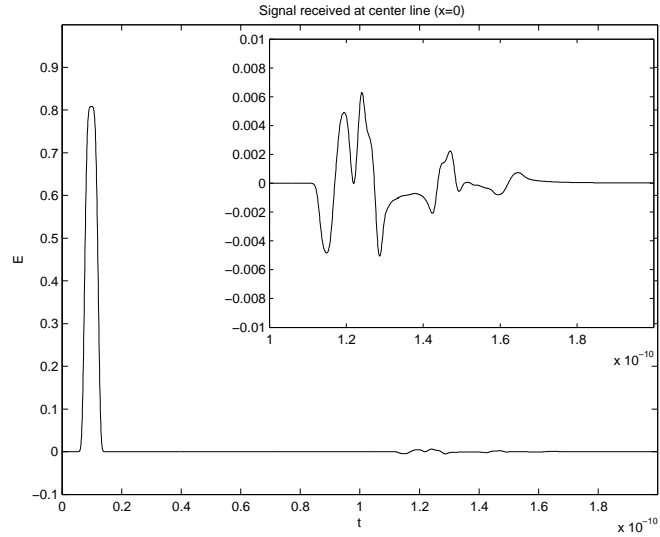

Figure 5: : Signal received at $x = 0$ on the center line for the case where the knit lines and surrounding regions are modeled separately (the inset is a magnification of the reflection).

8

4   Conclusions

We have developed a framework which accounts for the presence of knit lines in modeling the electromagnetic propagation of interrogating pulses in SOFI. We were able to compute, using classical electromagnetics formulations, estimates for the index of refraction in both the knit lines and the surrounding low-density foam based on measured values from time–of–flight experiments and observable material properties. The values were shown to be consistent with the laboratory based estimates that a 2% decrease in speed should be evident in the absence of knit lines.

In the effort to detect flaws in low–density materials such as foam, highly accurate models are required to give simulations the precision necessary to distinguish small amplitude reflections from noise, including that from model error. In particular, physics–based models have a foundation in theory, lending credibility and more importantly, reliability. To validate such models, it is necessary to compare predictions to experimental data. This validation process sometimes highlights short–comings, which require new physics to be developed.

The work herein provides an approach to enhance the accuracy of a model by making it more representative of the material in question, while at the same time not increasing substantially the computational complexity of the system to be solved. The results themselves suggest that knit lines should be taken into consideration in any precise modeling effort. But the approach of using the Clausius–Mossotti equation to augment the representation of the dielectric constant can also be applied more generally to other models. In particular, it is already being used to improve the performance of high–accuracy GPS measurement by accounting for the presence of water vapor in the air [5]. It is entirely possible that, rather than requiring a complicated distribution of *permittivities* to account for uncertainty due to the fluctuations in an otherwise homogeneous material, a simple distribution of *densities* may, through the Clausius–Mossotti equation, lead to a more accurate model of the variability in the dielectric parameters.

While the current formulation may be used as a forward solution in an inverse problem context, it is likely that the highest value will lie in its ability to generate synthetic data with which to test faster signal processing approaches to damage detection. Thus it can be used either to explore which shapes of voids are the hardest to detect, or to generate data for scenarios that are difficult or expensive to manufacture.

Future directions for this work include consideration of full Maxwell's equations with coupled polarization and/or scattering mechanisms to account for the attenuation observed in experiments. Further, in an actual experimental setup, the transmitter is some distance from the receiver, thus the plane wave enters the medium at a slight angle. Thus the delta distribution input used to define the antenna should be modified to lie along a slanted line.

Acknowledgements

References

[1] H. T. Banks, N. L. Gibson and W. P. Winfree, Gap detection with electromagnetic terahertz signals, Tech. Rep. CRSC-TR03-40, Center for Research in Scientific Computation, North Carolina State University, September, 2003; *Nonlinear Analysis: Real World Applications*, **6** (2005), 381–416.

[2] H. T. Banks and N. L. Gibson, Inverse problems involving Maxwell's equations with a distribution of dielectric parameters, Tech. Rep. CRSC-TR05-29, Center for Research in Scientific Computation, North Carolina State University, July, 2005; *Inverse Problems*, submitted.

[3] J. L. Johnson, T. D. Dorney and D. M. Mittleman, Enhanced depth resolution in terahertz imaging using phase-shift interferometry, *Appl. Phys. Lett.*, **78** (2001), 835–837.

[4] K. Carney, M. Melis, et al., Material modeling of space shuttle leading edge and external tank materials for use in the Columbia accident investigation, *Proceedings 8th International LS-DYNA Users Conference*, Dearborn MI, May 2-4, 2004.

[5] F. S. Solheim, J. Vivekanandan, R. H. Ware, and C. Rocken, Propagation delays induced in GPS signals by dry air, water vapor, hydrometeors, and other particulates, *J. Geophys. Res.*, **104**, **D8** (1999), 9663–9670.

[6] P. Wang, A. Beck, W. K orner, H. Scheller, and J. Fricke, Density and refractive index of silica aerogels after low- and high-temperature supercritical drying and thermal treatment, *J. Phys. D: Appl. Phys.*, **27** (1994), 414–418.

[7] D. L. Woolard, E. R. Brown, M. Pepper, and M. Kemp, Terahertz frequency sensing and imaging: A time of reckoning future applications?, *Proceedings of the IEEE*, **93**, **10** (2005), 1722–1743.

[8] J. Xu, et al., T-rays identify defects in insulating materials, Conference of Laser and Electro-Optics (CLEO) 2004, San Francisco, CA, May 2004.

[9] G. Zhao, M. Mors, T. Wenckebach, and P. Planken, Terahertz dielectric properties of polystyrene foam, *J. Opt. Soc. Amer. B*, **19** (2002), 1476–1476.

[10] H. Zhong, J. Xu, X. Xie, T. Yuan, R. Reightler, E. Madaras, and X.-C. Zhang, Nondestructive defect identification with terahertz time-of-flight tomography, *IEEE Sensors Journal*, **5** (2005), 203–208.